The effects of the Bragg curve on the nuclear track formation in CR-39 polycarbonate, with the atomic force microscopy approach

C. Vázquez-López[a], B.E. Zendejas-Leal[a], R. Fragoso[a], J.I. Golzarri[b], and G. Espinosa[b]
[a] *Departamento de Física. Centro de Investigación y de Estudios Avanzados del Instituto Politécnico Nacional, Av. IPN 2508, Col. San Pedro Zacatenco, 07360, México, D.F. México.*
Tel +5255 5747 3800 ext. 6108; Fax: +52 55 5747 3879
e-mail: cvlopez@fis.cinvestav.mx
[b] *Instituto de Física Universidad Nacional Autónoma de México. Circuito de la Investigación Científica, Ciudad Universitaria, 04520, México, D.F. México.*

Received 2 May 2012; accepted 9 January 2013

The etching nuclear track parameters were analyzed, using atomic force microscopy (AFM), allowing the simulation of the nuclear track profiles evolution. For these experiments, CR-39 (Lantrack^{TM}) was chosen, because the excellent energy response to alpha particles. Due to the AFM limitations, it was necessary to reduce the incident particle energy in order to reach the Bragg peak region in the AFM scanning process. The different profile shapes of the etched tracks were clearly observed in the evolution process.

Keywords: Etched nuclear track profiles; CR-39; atomic force microscope (AFM); etched nuclear track simulation; etched nuclear track evolution.

PACS: 24.40.Wk; 61.80.-x; 68.37.Ps

1. Introduction

In the interaction of incident ions with matter the Bragg-peak region appears to be of particular interest. Ions in this region are slowing down; their times of influence with electronic atomic shells are quickly increasing, as well as fluctuation of these interactions. It evokes drastic variations of the energy deposition rate that can be observed for dose or ionization rate, very related with the response of the detector material revealed as a nuclear track. The response of a dielectric detector is described by the function V(x), known as the particle registration sensitivity, which is defined as the ratio of track and bulk etch rates V_t/V_b. Its determination requires the measurement of both etching velocities separately by independent experiments. To measure the complete V function, the track evolution from the conical start phase near the sample surface down to the end of track around the Bragg peak has to be observed.

The Bragg curve effects in plastic detectors have been studied by means of confocal microscopy [1,2], holographic digital microscopy [3], and by cutting the sample nearly parallel to the track axis, and then using optical microscopy [4]. In these procedures the track features should be bigger than 1 μm, due to the optical wavelength limitations.

The topographical characterization of etched track may be also obtained by AFM, as has been reported by many authors [5-8]. The samples in all these studies are limited to the initial shape of the etched tracks, corresponding to conical cavities. In these samples the Bragg curve effects are not revealed, since the track registration parameter V_t is almost constant near the sample surface. In addition, there is a serious limitation in the AFM instrumentation that is necessary to remark: the topography of the sample should involve features with heights in the range between -3.5 and + 3.5 μm, corresponding to the larger available piezoelectric scanner actuator. Thus, the etched nuclear tracks should be smaller than 3.5 μm in length in order to be properly scanned by AFM.

In order to have the Bragg peak closer to the sample surface, in this work the procedure of reducing the incident particles energy has been employed, by separating the source from the target, in a similar way as that used in Ref. 4, who obtained attenuation by controlling the chamber pressure.

2. Experimental details

The AFM images were obtained with an Autoprobe CP Research (Thermomicroscopes, from Veeco Group) Instrument in the contact mode. The images were processed with the Pro Scan program, version 2.0, and complemented with the WSxM scanning probe software [9] All the experiments were performed with a piezoelectric scanner able to raster scan 100×100 microns in X-Y and $\pm$ 3.5 μm in Z scan range. Silicon Veeco cantilever of 45 microns in thickness with 0.2 N/m spring constant supported the tip. The tip-sample force was kept constant at 10^8 N. All the measurements were carried out in air, at room temperature (20°C), and with a raster scan frequency of 0.5 and 1 Hz. The tip was of the ultralever type, with a curvature radius of 100 Å.

CR-39 Lantrack (9×19 mm chips) of 600 microns thickness was used as detecting material. A plutonium (^{239}Pu) emitter of 5.15 MeV alpha particles was selected as the track generator radioactive source. The exposure was made in air, at different distances between the source and the detector. For an analysis by AFM it was necessary to obtain a high track density of alpha particles. In this case the material was exposed to have 10^6 tracks per cm^2.

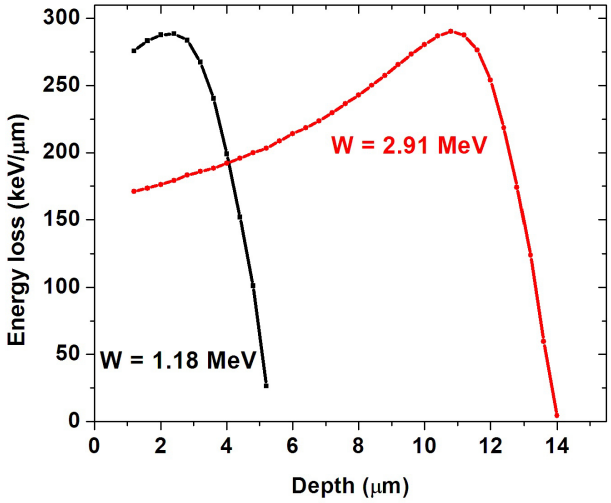

FIGURE 1. Bragg curves for alpha particles emitted by a ^{239}Pu source, on a CR-39 plastic target at 20 and 30 mm distance, whose incident energies are: 2.91 MeV, and 1.18 MeV, respectively.

All the detectors were chemically etched under the same conditions in an ultrasonic bath, in 6.0 M KOH solution at 60 $\pm$ 1°C, at different etching times. The detectors reported in this work were exposed to the alpha source at two distances: 2 and 3 cm. The SRIM calculation [10], whose results are shown in Fig. 1 revealed alpha incident energies W of 2.91 MeV for the former distance and of 1.18 MeV for the second one. The particle ranges R were 13.5 μm for W = 2.91 MeV and 4.94 μm for W = 1.18 MeV. The thickness of each detector was measured before and after each etching, such that the bulk etching speed was monitored during the etching, resulting V_b = 1.23 μm/h. The full set of detectors was washed and dried with the same process and conditions. After these procedures, the detectors were scanned with the AFM.

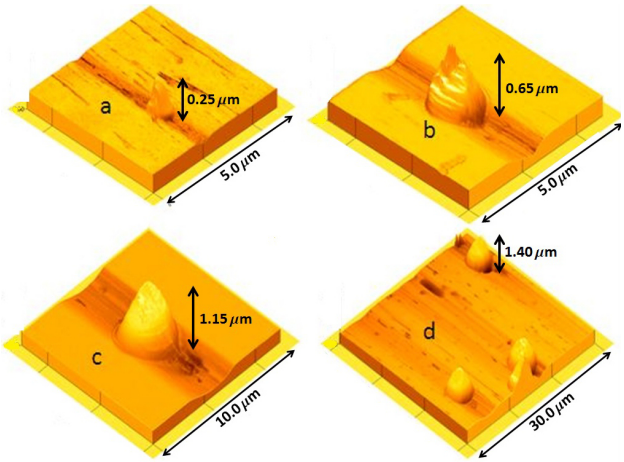

FIGURE 2. Inverted 3-d AFM images of samples irradiated at 2 cm distance from the ^{239}Pu source.

3. Results and discussion

In Fig. 2 four representative 3-d AFM images are shown. In this work the 3-d images were vertically inverted for the sake of appreciation of the difference between them. These samples were exposed to alpha particles with W = 2.91 MeV, and etching times of 0.5, 2.0, 3.0, and 4.0 h, respectively. In Fig. 3 the corresponding 3-d images for the samples exposed to alpha particles of 1.18 MeV are shown. The samples were etched during 0.5, 1.0, 1.5, and 2 h, respectively. The last image clearly shows the typical morphology of the over-etched tracks.

In Fig. 4 the etching time dependence of the track lengths are shown. For the 1.18 MeV irradiated samples a saturation of L(t) occurs at 2 hours of chemical etching. The saturation time is 2 hours in this case. For each etching time the optical microscope attached to the AFM system was used to choose at least five of the pits to be scanned. Then profiles along representative cross section lines were determined for each

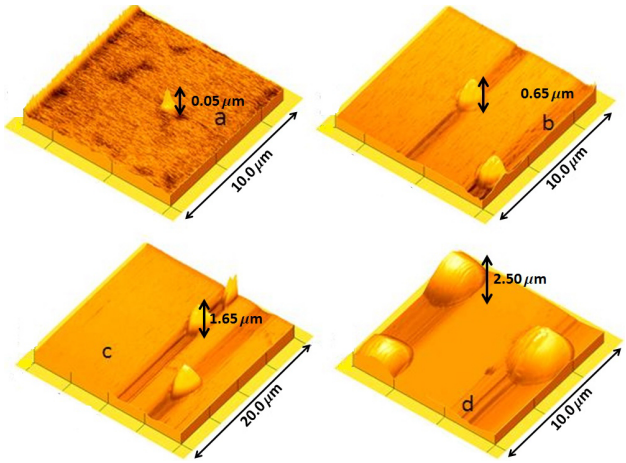

FIGURE 3. Inverted 3-d AFM images of samples irradiated at 3 cm distance from the ^{239}Pu source.

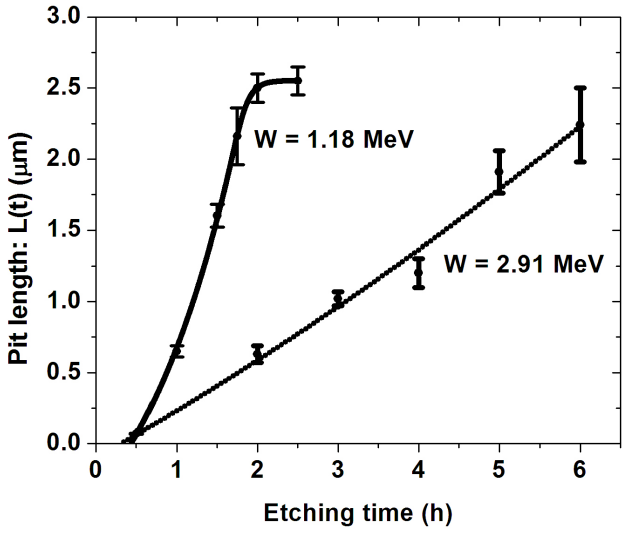

FIGURE 4. Pit length $L(t)$ as a function of the etching time.

chosen pit in the image analysis process, and the average as well as the standard deviation of the pit lengths was calculated. The standard deviation is represented by error bars.

Following Dörschel and Hermsdorf, the vertex position of the track along the track axis is determined by: [4]

$$X(t) = V_b t + L(t) \tag{1}$$

Where $X(t)$ is the track vertex position, measured from the detector original surface.

Equation (1) with $L(t)$ expressed as piece wise interpolation of continuous functions, was also used to establish the track vertex position in the numerical integration.

The track etch rate is given by:

$$dX/dt = V_t = V_b + dL/dt \tag{2}$$

The set of data $\{dL/dt$ vs $t\}$ were numerically obtained from $L(t)$ graphs, and conveniently smoothed. In the worksheet of data there should be a column of etching times in seconds, a column of $L(t)$ in nm, and a column of dL/dt. A fourth column of $X = V_b$t + L(t) should be calculated. A fifth column of $V = 1 + (dL/dt)/V_b$ should also be calculated. Then the data of columns X and V are used to graph V versus X, resulting in the graphs shown in Fig. 5.

For the special case of a perfectly conical track the vertex angle θ is related with the parameter V by [11]:

$$V = 1/\sin\theta, \tag{3}$$

In Fig. 6 a general track profile is sketched. In this case θ is a position dependent function as indicated. At an arbitrary point x, $V(x)$ is associated with the angle $\theta(x)$ by:

$$V(x) = 1/\sin\theta(x) \tag{4}$$

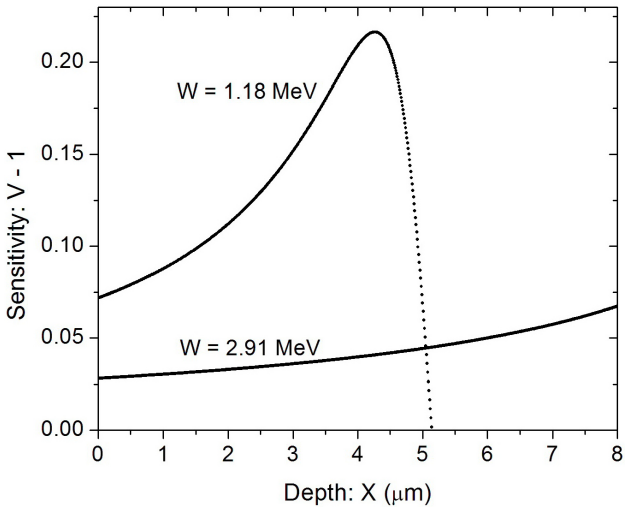

FIGURE 5. The track registration sensitivity $V - 1$ as a function of depth.

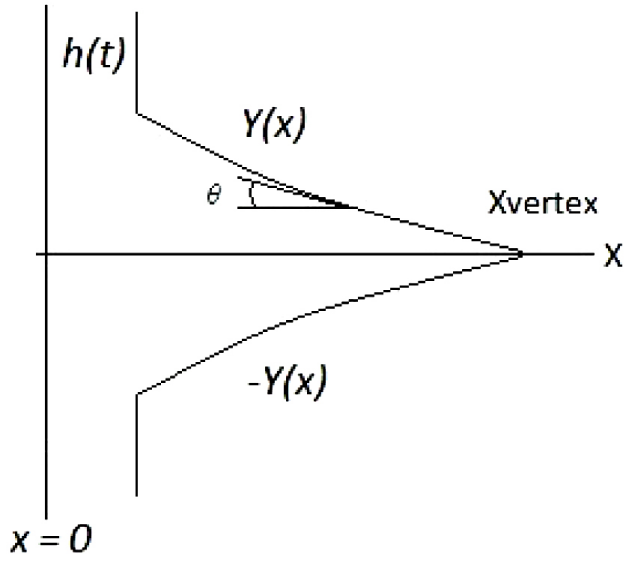

FIGURE 6. Sketch of the track profile. The distance to the original surface $h = V_b t$ corresponds to the dissolved material.

The x-dependence will be understood from now on.

From Eq. 4, $\tan(\theta)$ = 1/Sqrt(V^2 - 1). Then the x-dependence slope of the etched track profile is given by:

$$dY(x,t)/dx = -1/\text{Sqrt}(V^2 - 1) \tag{5}$$

Where $Y(x,t)$ is the track profile function and t is the etching time, as shown in Ref. 12.

Thus our goal is to solve Eq. 5 with the appropriated integration constant. The function Y evaluated at the etched track vertex should be zero:

$$Y(X_{\text{vertex}}, t) = 0 \tag{6}$$

Thus the integration constant is determined by Eq. 6, such that the track profile function evaluated at any point in the range $0 < x \leq X_{\text{vertex}}$ is determined by the area under the curve:

$$Y(x,t) = \text{Area}(x) - \text{Area}(X_{\text{vertex}}) \tag{7}$$

Which is equivalent to:

$$Y(x,t) = \int_x^{x_{\text{vertex}}} \frac{dx'}{\sqrt{V^2(x') - 1}} \tag{8}$$

Which has to be integrated numerically.

The over-etched tracks are defined by $V(x) = 1$, fulfilled for $x \geq R$, where R is the particle range, and then Eq. (8) is not longer valid. The etching process ratio in this case is V_b in the whole cavity wall. These tracks have profiles obtained from the track whose vertex is located at R. This track is defined as the saturation track profile. It is possible to use the Huygens principle to obtain geometrically the evolution of the over-etched tracks, as Bondarenko *et al.*, reported [13]. Each point on the track contour is considered as belonging to the circular front of the etching process. That front spreads from a certain point of the saturation track profile. The speed of front spreading equals the etching speed V_b in bulk. In

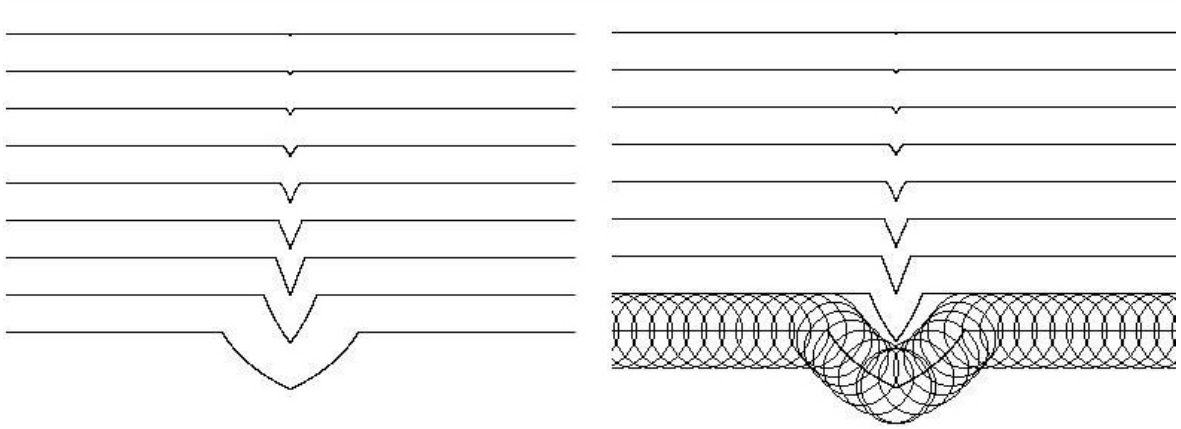

FIGURE 7. Huygens procedure for the calculus of an over-etched track.

Fig. 7 this procedure is indicated. Let us call the set $\{(x_s, Y_s)\}$ as those points corresponding to the saturation track profile as sketched by the bottom profile at the left hand side of Fig. 7. Then an over-etched track profile is given by the generation of circles whose centers are located at (x_s, Y_s), and the radius is given by:

$$\Delta h = (t - \text{SaturationTime}) * V_b \tag{9}$$

The over etched track is the external contour of the circles family. This geometrical approach is equivalent to the following transformations:

$$(x_s, Y_s) \rightarrow (x_s + \text{phase}X, Y_s + \text{phase}Y), \tag{10}$$

where $\text{phase}X = \Delta h * \sin\theta$ and $\text{phase}Y = \Delta h * \cos\theta$, which in turn:

$$\sin\theta = 1/V(x_s) \quad \text{and} \quad \cos\theta = \frac{\sqrt{V^2(x_s) - 1}}{V(x_s)}, \tag{11}$$

In Fig. 8, the evolution of the track profiles corresponding to W = 2.91 MeV is shown. In this calculation the etching time between neighbor profiles is 10 minutes. The conical shape does not depend on the etching time. Then the influence of the Bragg peak is not present, as expected. As mentioned above, the particle range is 13.5 μm, and the pit length necessary to reach the end of the latent track is larger than 3.5 μm.

In Fig. 9 the evolution of the etched track is shown, in which the source to target distance is 3 cm. For comparison, in this figure the scale is the same as that of Fig. 8. In this case the track shapes reveal the influence of the Bragg curve: The etched tracks are larger than those of Fig. 8. In the tenth and eleventh profiles, after 1.7-hour etching time, convex cavities are observed, as corresponds to a high increase of energy loss ratio of the alpha particle, just before the Bragg peak. In the twelfth profile the cavity is partially concave, which corresponds to a sharp decrease of the energy loss ratio of the incident ion, just after the Bragg peak. The last five profiles correspond to over-etched tracks.

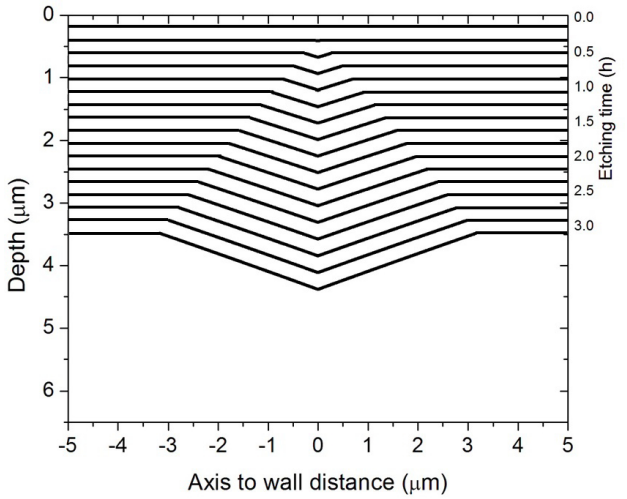

FIGURE 8. Evolution of the track profiles corresponding to W = 2.91 MeV. The etching time scale corresponds to the horizontal CR-39 surface.

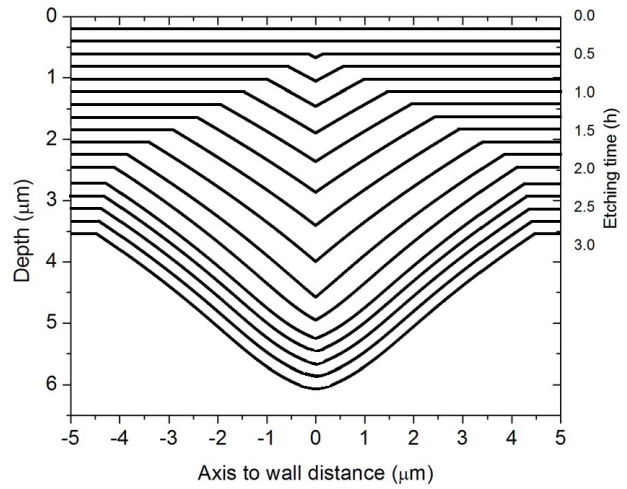

FIGURE 9. Evolution of the track profiles corresponding to W = 1.18 MeV. The deeper five profiles are over-etched tracks. The etching time between tracks is 10 minutes. The etching time scale corresponds to the horizontal CR-39 surface.

4. Conclusion

Atomic Force Microscopy was used to obtain etched nuclear track images and to determine their 3-dimentional shapes. Using these data, a numerical simulation was performed based on the etching time dependence of the pit length $L(t)$ and on the position dependence track registration sensitivity $V(x)$. In order to observe the Bragg curve effects using AFM, the incident particle energy was attenuated to 1.18 MeV by separating the Pu source from the target a distance 3 cm. The different profile shapes known to appear during track etching were clearly observed.

Acknowledgments

This work was partially supported by Instituto de Ciencia y Tecnología del Distrito Federal, México, grant 325-2009, and PAPIIT-DGAPA-UNAM Projects IN101910 and IN103013.

1. F. Vaginay, M. Fromm, D. Pusset, G. Meesen, A. Chambaudet, and A. Po, *Rad. Meas.* **34** (2001) 123.
2. D.Hermsdorf, *Rad. Meas.* **44** (2009) 806.
3. F. Palacios, J. Ricardo, D.Palacios, E. Goncalves, J. Valin, and R. De Souza, *Optics Comm.* **248** (2005) 41.
4. B. Dörschel, D. Hermsdorf, U. Reichelt, S. Starke, *Radiat. Meas.* **37** (2003) 573.
5. G. Espinosa, I. Jacobson, J. I. Golzarri, C. Vázquez, R. Fragoso, and E. Santos, *Rad. Protect. Dosimetry.* **101** (2002) 89.
6. M. Yamamoto *et al.*, *Rad. Meas.* **28** (1997) 227.
7. N. Yasuda, M. Yamamoto, N. Miyahra, N. Ishigure, T. Kanai, and K. Ogura, *Nucl. Inst. Meth. In Phys. Res. B* **142** (1998) 111.
8. D. Nikezic, J.P.Y. Ho, C.W.Y. Yip, V.S.Y. Koo,and K. N. Yu, *Nucl Inst Meth in Phys Res B.* **197** (2002) 293.
9. I.Horcas, R. Fernández, J.M. Gómez-Rodríguez, J. Colchero, J. Gómez-Herrero, and M. Baro, *Rev. Sci. Instrum.* **78** (2007) 013705. This software is free and available in www.nanotec.es site.
10. J.F. Ziegler, J.P. Biersack, and U. Littmark, *The Stopping and Ranges of Ions in Solids* (Pergamon Press, Oxford, 1985). The code is available in http://www.srim.org.
11. G. Somogyi, *Nucl Instrum and Meth* **173** (1980) 21.
12. D. Nikezic and D. Kostic, *Radiat. Meas.* **28** (1997) 185.
13. Î.À. Bondarenko, D.V. Melnichuk, Yu.N. Onishchuk, S.Yu. Medvedev, Morphologic analysis of SSNTD tracks based on the Huygens principle for the purpose of alpha spectrometry. https://www.jiscmail.ac.uk/.